


---

This is the **accepted version** of the journal article:

Saraza-Canflanca, Pablo; Castro-Lopez, Rafael; Roca, Elisenda; [et al.].  
«Determination of the time constant distribution of a defect-centric time-  
dependent variability model for Sub-100-nm FETs». IEEE Transactions on  
Electron Devices, Vol. 69, issue 10 (Oct. 2022), p. 5424-5429. 6 pàg. DOI  
10.1109/TED.2022.3198383

---

This version is available at <https://ddd.uab.cat/record/283766>

under the terms of the  **CC BY** COPYRIGHT license

# Determination of the time constant distribution of a defect-centric Time-Dependent Variability model for sub-100nm FETs

P. Saraza-Canflanca, R. Castro-Lopez, E. Roca, J. Martin-Martinez, R. Rodriguez, M. Nafria, F. V. Fernandez

**Abstract**—The origin of some Time-Dependent Variability phenomena in FET technologies has been attributed to the charge carrier trapping/de-trapping activity of individual defects present in devices. Although some models have been presented to describe these phenomena from a so-called defect-centric perspective, limited attention has been paid to the complex process that goes from the experimental data of the phenomena up to the final construction of the model and all its components, specifically the one that pertains to the time constant distribution. This paper presents a detailed strategy aimed at determining the defect time constant distribution, specifically tailored for small area devices, using data obtained from conventional characterization procedures.

**Index Terms**—BTI, Characterization, FET devices, Modeling, Time-Dependent Variability

## I. INTRODUCTION

TIME-DEPENDENT-VARIABILITY (TDV) phenomena in FET technologies, such as Bias Temperature Instability (BTI) or Random Telegraph Noise (RTN), have been a subject of increasing attention [1]. A widely accepted hypothesis to explain the origin of these phenomena is the capture/emission of charge carriers in/from defects in the field-effect transistor, which, in small area devices, induce discrete shifts in the transistor threshold voltage and, these, in turn, cause discrete drain current shifts [2]. The parameters associated with the defects, namely the emission and capture times as well as the induced threshold voltage shifts, do not have the same value for all defects. Rather, their values follow probability distributions. Defect-centric models, such as the Probabilistic Defect Occupancy (PDO) model [3], have been proposed to account for the stochasticity of TDV phenomena in deeply-scaled technologies. Determination of the distribution of amplitude shifts has been dealt with in previous literature [4]–[6]. This paper focuses on how to determine, from experimental data, the distributions followed by the time constants of the defects, i.e., the capture/emission time (CET) maps [7].

To this end, a statistical analysis of the individual defects has

been proposed [7], for instance, by making use of time-dependent defect spectroscopy (TDDS) [8]. High gate voltages are applied many times (e.g., 100) under the same voltage and timing conditions. The tracking of each defect (identified by the amplitude of the current shift) is performed to get the average times at which a charge is emitted and, thus, extract the corresponding emission time constant ( $\tau_e$ ). This fact alone dramatically limits the range of time constants that can be accurately obtained to a small fraction of the experimental window. The reason for this is that the exact time at which a charge is actually emitted, i.e., its time-to-emission, can be anywhere in the range of several decades around the time constant value [9]. The defects with time constants that are not sufficiently below the upper limit of the experimental window may not undergo an emission event within the experimental timeframe in some of the repeated experiments described above. Therefore, the accuracy of the determination of such time constant decreases dramatically. A similar problem occurs if the time constant of the defect is not sufficiently above the lower limit of the experimental window. In summary, this approach finds difficulties in properly building the CET map because only a fraction of the defects would be accurately identified. Moreover, the approach is also very lengthy and prone to errors, since different defects with similar amplitudes could be mistaken for one another.

An alternative solution was proposed in [7] and later developed in [10]–[12]: to match the integral of the CET map multiplied by the probability of occupation to the recovery traces of the threshold voltage of large devices, which contain hundreds or thousands of defects. To carry out this matching, an average threshold voltage shift and an average number of defects are considered. Although these works show a good result for the averaged impact of many defects in large devices, their ability to describe the experimental stochastic distributions of the phenomena in small area devices has not been yet demonstrated. In other words, there can be many combinations of distribution functions that account for the macroscopic averaged current degradation and recovery in large devices but that do not match the stochastic behavior in small devices.

This work was supported by grants PID2019-103869RB-C31 and PID2019-103869RB-C32 funded by MCIN/AEI/10.13039/501100011033, and by Consejería de Economía, Conocimiento, Empresas y Universidad de la Junta de Andalucía and P.O. FEDER under project US-1380876. P. Saraza-Canflanca, R. Castro-Lopez, E. Roca and F. V. Fernandez

are with Instituto de Microelectrónica de Sevilla (Universidad de Sevilla, CSIC), Sevilla, Spain (email: [Francisco.Fernandez@imse-cnm.csic.es](mailto:Francisco.Fernandez@imse-cnm.csic.es)). J. Martin-Martinez, R. Rodriguez and M. Nafria are with the Department of Electronic Engineering, Universitat Autònoma de Barcelona, 08193, Bellaterra, Spain.

This paper vindicates a method to determine the capture/emission time maps that is able to describe the stochastic behavior of small transistors from the experimental statistical study of such small transistors. Unlike previous approaches, (a) identification of the same individual defect across different experiments is not necessary, (b) the actual times at which emission events occur are accounted for, and (c) the experimental statistical distributions of times-to-emissions in recovery traces of small area devices are perfectly matched.

## II. CHARACTERIZATION STRATEGY

In the following, the employed measurement technique has been the well-known Measure-Stress-Measure (MSM) one [13], using the transistor array in [14] and the experimental setup in [15]. First, 600 pristine PMOS devices of  $W=80\text{nm}$  and  $L=60\text{nm}$  fabricated in a 1.2-V 65-nm CMOS technology are measured (i.e., before any stress voltage is applied) to obtain a reference. Then, 5 stress-measure cycles are applied to each device with exponentially increasing stress times between 1s and 10,000s. In the stress phases, the devices are biased with voltages over the nominal value ( $|V_{gs}| = 2.5\text{V}$ ) to enable the so-called accelerated aging, during which charges are expected to get trapped into defects. In the recovery phases, the devices are biased below their nominal conditions ( $|V_{gs}| = 0.6\text{V}$  and  $|V_{ds}| = 0.1\text{V}$ ) and their drain current is measured for 100s. In these phases, charges are expected to get de-trapped from the defects. These de-trapping events are observed as sudden and discrete increases in the drain current, as can be seen in the experimental trace example in Fig. 1a. As it will be explained in the next Section, the time instants at which these de-trapping events occur,  $t_e$ , will be used to investigate the distribution of the time constants of the defects. In particular, only Single Emission Events (SEE) will be considered, being a SEE an emission of a charge from a defect if, later in the measurement window, such defect does not capture another charge. This is a normal practice in BTI characterization and does not imply a significant limitation. The only alternative emission/capture events that

can appear in a current trace are illustrated with the experimental trace example in Fig. 1b. It can be seen that, together with several SEEs, a defect shows multiple charge trapping and de-trapping events. This is a defect that manifests as Random Telegraph Noise (RTN) at the low gate and drain voltages applied during the recovery phase. Therefore, it is not convenient to consider them during the parameter extraction procedure based on MSM since it would unnecessarily complicate the mathematical formulation.

From the current traces, defect information is extracted using a Maximum Likelihood Estimation (MLE)-based method [16]. MLE estimates the parameters of a statistical model for the current levels of the experimental trace given the measured current samples. The background noise can be approximated by a Gaussian distribution which is independent of the different current levels induced by the threshold voltage shifts associated to charge carrier trapping/detrapping. Then, the measured current trace can be considered as samples of a probability density function (pdf) formed by the addition of different Gaussian distributions centered at the different current levels:

$$f(I|\theta) = \frac{1}{K\sqrt{2\pi\sigma^2}} \sum_{j=1}^M A_j e^{-\frac{(I-I_{Lj})^2}{2\sigma^2}} \quad (1)$$

where  $\theta$  is the vector of parameters of the probability density function,  $\sigma$  represents the standard deviation of the background noise,  $I_{Lj}$  is the value of each of the  $M$  current levels,  $A_j$  the value of its distribution height, and  $K$  a normalization constant so that the area below the pdf is unity.

The MLE method tries to identify the parameter values  $\theta$  that make the measured data  $\{I_1, \dots, I_N\}$  the most probable, which can be easily formulated and solved as an optimization problem. Once the  $M$  discrete current levels have been identified, the next step is to generate a clean or background-noise-free current trace from the experimental one. For this, the current value of the closest of the  $M$  current levels is assigned to each experimental current point.

In the present case, defects that do not undergo a single emission event (i.e., defects that undergo both trapping and detrapping events, which induce current shifts of equal amplitude but opposite sign, as those in Fig. 1b) are removed from the clean trace, and only recovery detrapping events are left. With the experimental setup used [15] and this extraction algorithm, detrapping events with amplitudes down to 1.7nA have been detected. From the resulting clean recovery trace, the emission time instants ( $t_e$ ) and amplitudes of SEEs ( $\Delta I_D$ ) can be directly extracted.

## III. THEORETICAL BACKGROUND

To analytically tackle the occurrence of a SEE during a measurement window, two fundamental requirements must be considered: (a) the defect must exist and be already occupied at the beginning of the recovery phase, and (b) it must undergo an emission during the measurement window without undergoing a capture event for the rest of the measurement window. These two requirements are mathematically formulated in the following.

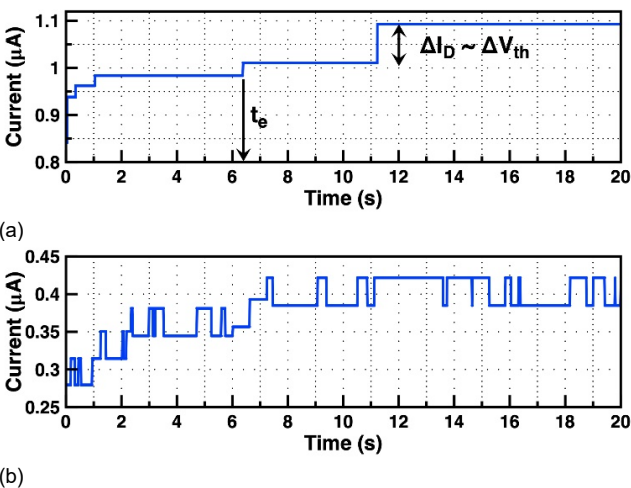


Fig. 1. Examples of experimental current trace in a recovery phase: (a) containing only SEEs and (b) containing SEEs and RTN trapping/detrapping events. Examples of time-to-emission and current shift of an SEE are marked with arrows.

### A. Requirement 1: The defect exists and is occupied at the start of the recovery phase

The probability that a defect characterized by a given pair of time constants ( $\tau_e$ ,  $\tau_c$ ) exists is determined by the probability density function  $P_{def}$ . In this work, a bivariate lognormal distribution has been considered [17]:

$$P_{def}(\tau_e, \tau_c) = \frac{1}{2\pi\tau_e\tau_c\sigma_{\tau_e}\sigma_{\tau_c}\sqrt{1-\rho^2}} \cdot e^{-\frac{1}{2(1-\rho^2)}\left[\frac{(l\tau_e-\mu_{\tau_e})^2}{\sigma_{\tau_e}^2} + \frac{(l\tau_c-\mu_{\tau_c})^2}{\sigma_{\tau_c}^2} - \frac{2\rho(l\tau_e-\mu_{\tau_e})(l\tau_c-\mu_{\tau_c})}{\sigma_{\tau_e}\sigma_{\tau_c}}\right]} \quad (2)$$

where  $l\tau_e = \log(\tau_e)$  and  $l\tau_c = \log(\tau_c)$ . Parameters  $\mu_{\tau_e}$  and  $\mu_{\tau_c}$  are the mean values of the emission and capture times' logarithm,  $\sigma_{\tau_e}$  and  $\sigma_{\tau_c}$  are the standard deviations and  $\rho$  is the correlation coefficient. An example of such distribution is represented in Fig. 2a for the set of model parameter values obtained in Section IV and indicated in Table II. Note also that time constants depend on the applied gate and drain biasing voltages [18]. The following exponential dependencies on the gate and drain voltages are assumed (with source and bulk short-circuited):

$$\begin{aligned} \tau_e &= \tau_{e0} 10^{\beta_e(|V_{gs}| - |V_{gsref}|)} 10^{\gamma_e(|V_{ds}| - |V_{dsref}|)} \\ \tau_c &= \tau_{c0} 10^{\beta_c(|V_{gs}| - |V_{gsref}|)} 10^{\gamma_c(|V_{ds}| - |V_{dsref}|)} \end{aligned} \quad (3)$$

The absolute values have been used for the voltages so that they take positive values for pMOS transistors. These voltage dependencies are common in the literature and fit well with the experimental measurements [18]. Parameters  $\tau_{e0}$  and  $\tau_{c0}$  correspond to the time constants for  $|V_{gs}| = |V_{gsref}|$  and  $|V_{ds}| = |V_{dsref}|$ . Here, we consider the reference voltages as those used during the recovery phase. Then, the distribution in (2) is evaluated at these voltages, so that  $\tau_e = \tau_{e0}$  and  $\tau_c = \tau_{c0}$ , as depicted in Fig. 2a. In addition, the proposed method for the determination of the time constant distribution can also be applied in case a different mathematical formulation of the distribution function in (2) is proposed.

To undergo a SEE, the defect must be occupied at the beginning of the recovery phase. This can be evaluated through the probability of occupation function ( $P_{occ}$ ) [2], which provides the probability that a defect is occupied for a given biasing condition and time. Although only the  $P_{occ}$  at the beginning of each recovery phase is needed, it is necessary to evaluate its evolution throughout all previous stress-measure phases.  $P_{occ}$  can be formulated in differential form as [19]:

$$\frac{dP_{occ}(t)}{dt} + P_{occ}(t) \left( \frac{1}{\tau_e} + \frac{1}{\tau_c} \right) - \frac{1}{\tau_c} = 0 \quad (4)$$

Then, since the exact timing and biasing conditions of each stress-measure phase are known, it is possible to easily solve (4) analytically to obtain the evolution of  $P_{occ}$  at each phase. Indeed, when solving (4), time constants ( $\tau_e$ ,  $\tau_c$ ) must be calculated according to (3) for each phase. For the sake of illustration, Fig. 2b displays the  $P_{occ}$  distribution at the end of one of the stress cycles. The product of the distributions in Fig. 2a and Fig. 2b, illustrated in Fig. 2c, yields the probability of existence of charged defects at the end of one stress phase that

could potentially produce a SEE during the subsequent recovery phase. The voltage coefficients in (3) can vary from defect to defect. In this paper, we will consider the mean value of such dependences.

### B. Requirement 2: The defect undergoes a SEE

As defined above, a SEE implies an emission event during the measurement window that is not followed by a capture event. Since the emission of a charge from a defect can be modeled as a Markov process [20], the probability that a defect characterized by an emission time constant  $\tau_e$  emits a charge at time  $t_e$  is given by [19]:

$$P_{emi}(t_e|\tau_e) = \frac{1}{\tau_e} e^{-t_e/\tau_e} \quad (5)$$

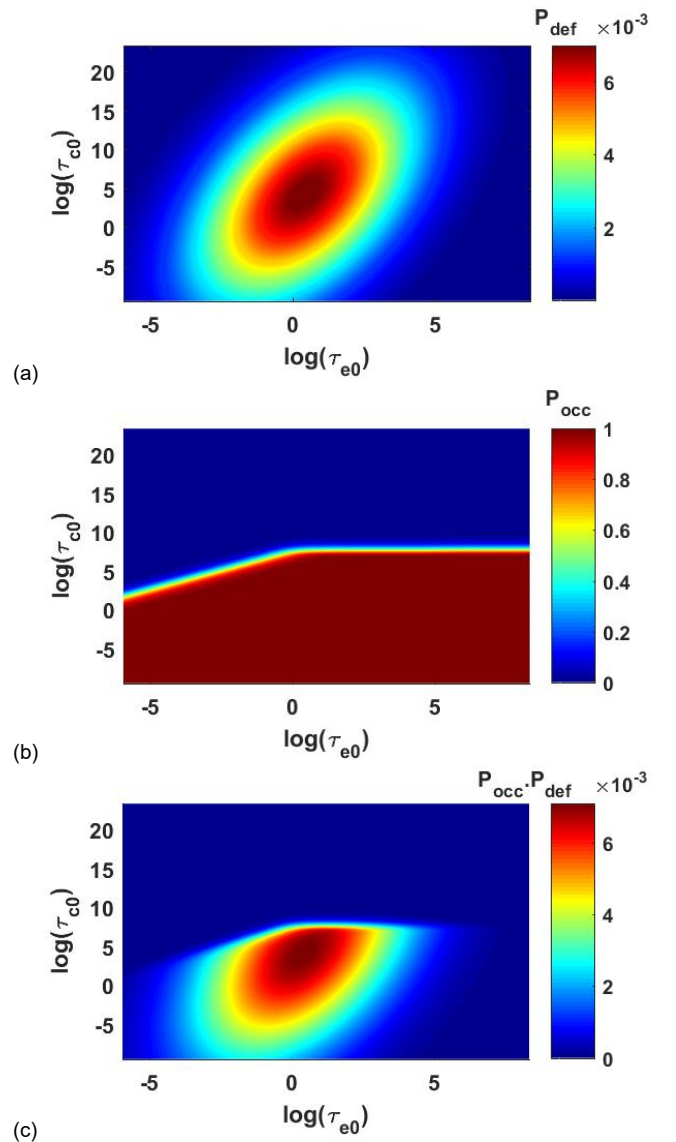


Fig. 2. An example of (a) a bivariate lognormal distribution of the defect time constants, (b) a probability of occupation of the defects after the stress cycle of 1000s, (c) a distribution of charged defects at the end of the stress period.  $\tau_{e0}$  and  $\tau_{c0}$  are referred to  $|V_{gsref}| = 0.6V$  and  $|V_{dsref}| = 0.1V$ . Decimal logarithm has been used in all plots in this paper.

Analogously, the probability that the defect, characterized by a capture time constant  $\tau_c$ , captures a charge at a given time  $t$  after it has emitted one at time  $t_e$  is given by:

$$P_{cap}(t|t_e, \tau_c) = \frac{1}{\tau_c} e^{-\frac{t-t_e}{\tau_c}} \quad (6)$$

The probability that the charge is captured between  $t_e$  and the end of the measurement window  $t_{max}$  is given by the definite integral of (6) between these limits. And vice versa, the probability that a defect, with capture time constant  $\tau_c$ , does not capture a charge, after emitting one at  $t_e$ , before the end of the measurement window  $t_{max}$  will be given by one minus such definite integral:

$$P_{nocap}(t_e|\tau_c) = 1 - \int_{t_e}^{t_{max}} \frac{1}{\tau_c} e^{-\frac{t-t_e}{\tau_c}} dt = e^{-\frac{t_{max}-t_e}{\tau_c}} \quad (7)$$

Then, it must be considered that the measurement window has a lower limit  $t_{min}$  (experimentally, this limit is, at least, the sampling rate of the current measurement instrument which, in this case, is 2ms), i.e., assuming that measurement procedures have started just after the recovery begins, SEEs happening below time  $t_{min}$  of the recovery period will not be detected. During the measurement window, bounded by  $t_{min}$  and  $t_{max}$ , the probability that a defect with certain time constants ( $\tau_e, \tau_c$ ) experiences a detectable SEE is given by the product of (5), i.e., the defect emits a charge, and (7), i.e., the defect does not capture a charge before  $t_{max}$ :

$$P_{see}(t_e|\tau_e, \tau_c) = P_{emi}(t_e|\tau_e) \cdot P_{nocap}(t_e|\tau_c) \quad (8)$$

And, therefore the probability to detect a SEE at any time instant is:

$$P_{see}(t_e|\tau_e, \tau_c) = \begin{cases} 0 & t_e < t_{min} \\ \frac{1}{\tau_e} e^{-\frac{t_e}{\tau_e}} e^{-\frac{t_{max}-t_e}{\tau_c}} & t_{min} \leq t_e \leq t_{max} \\ 0 & t_e > t_{max} \end{cases} \quad (9)$$

Again,  $\tau_e$  and  $\tau_c$  in (9) must be calculated according to (3). Since SEEs occur during the recovery phase and the reference voltages have been considered as those of the recovery phase,  $\tau_e = \tau_{e0}$  and  $\tau_c = \tau_{c0}$  in (9).

### C. SEE observation probability

Finally, to detect a SEE, the defect, characterized by its time constants  $\tau_e$  and  $\tau_c$ , must be charged at the end of the stress phase (i.e., beginning of the recovery phase) and a SEE must occur during the measurement window. Mathematically, this is given by the product of (2), the solution of (4), and (9):

$$P_{labsee}(t_e, \tau_e, \tau_c) = P_{def}(\tau_e, \tau_c) \cdot P_{occ}(t = t_0) \cdot P_{see}(t_e|\tau_e, \tau_c) \quad (10)$$

where  $t_0$  is the time instant at which the recovery phase starts.

At the laboratory, only the time instants  $t_e$  at which SEEs occur can be measured. Actually, since they are statistically

distributed, their cumulative distribution function (Fig. 2) can be calculated. Mathematically, it is possible to obtain the probability density function by integrating the three-dimensional distribution in (10) for every possible value of  $\tau_e$  and  $\tau_c$ :

$$P_{lab\_vis\_te}(t_e) = \iint P_{labsee}(t_e, \tau_e, \tau_c) d\tau_e d\tau_c \quad (11)$$

The cumulative density function (cdf) can be easily obtained from the integration of equation (11), and this cdf will be fitted to the experimental cdf data, to determine the defect distribution in (2), as described in the next section. Notice that, unlike conventional approaches, there is no need to track individual defects in many MSM experiments on the same devices to determine their averaged time constants from the observed time-to-emissions. As discussed in Section I, this would limit, dramatically, the usability of the emission events observed in the laboratory to fit the time constant distribution. However, with the proposed approach, the distribution of time-to-emissions is directly fitted and, hence, every single emission event observed in the laboratory is effectively used in the fitting procedure.

## IV. FITTING OF EXPERIMENTAL DATA

Red square symbols in Fig. 3 show the experimental cdf of the time instants at which SEEs are observed (i.e.,  $t_e$ ) for the 5 MSM cycles of the characterization of 600 PMOS devices described in Section II. Table I shows the mean and variance of the number of SEEs detected per PMOS device at each of the five recovery cycles of the MSM procedure.

To illustrate the proposed methodology, the defect time constant distribution that describes the time-to-emission distributions in Fig. 3 will be built. Note that, though the shape of the distributions is very similar, as expected, they are shifted towards larger emissions times with the stress time. The model parameters in (2) have been adjusted so that the cdf corresponding to (11) best fits the experimental SEEs in Fig. 3. The drain-source voltage  $V_{ds}$  has practically no change in this experiment; hence, the drain voltage dependence of the time constants can be neglected. The fitting is performed by minimizing the difference between both cdfs using Particle Swarm Optimization, a global optimization algorithm that does not require any initial estimate of the fitting parameters [21]. Its application yields the values of the distribution parameters for our case study in Table II. Notice that the mean and standard deviations correspond to a log-time scale and as such they are dimensionless. As stated in Section III, they are referred to the drain and gate reference voltages. The corresponding defect distribution is shown in Fig. 2a. Only a portion of the defects modeled by this distribution manifests as SEEs during the

TABLE I  
MEAN AND VARIANCE OF THE NUMBER OF SEES PER DUT DETECTED AT EACH RECOVERY CYCLE

Cycle	1	2	3	4	5
Mean	1.355	1.742	2.151	2.502	2.926
Variance	1.447	1.993	2.233	2.810	3.371



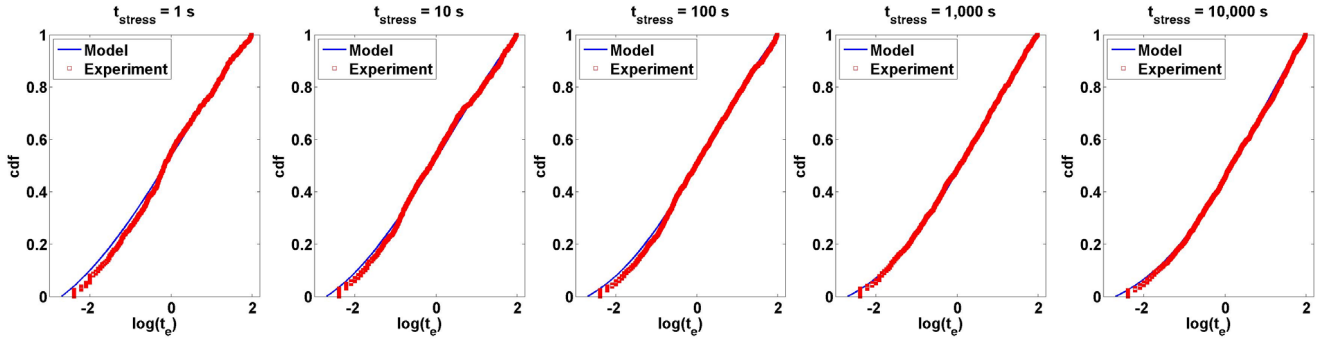


Fig. 3. Comparison of cdf of time of SEEs detected for 600 devices stressed at  $|V_{gs}| = 2.5V$ , for a recovery phase of 100s, and the representation of the cdf corresponding to (11) for the 5 SM cycles using the bivariate lognormal distribution in (2) with the parameters in Table II.

experimental window. Fig 4 shows the pdf in (11) for the 5 SM cycles using the time constant distribution in Table II.

Fig. 3 (continuous blue line) shows the representation of the cdf obtained from (11). A normalization factor has been applied to the cdfs so that they can be meaningfully compared to the experimental cdfs. Indeed, to get consistent optimization results, the normalization factor of the cdf is imposed to be the same for all cycles. It can be seen that there is an excellent

agreement with the experimentally observed SEEs. Note that the differences between the simulated cdf and the experimental cdf are slightly larger for the first two plots. This is an expected statistical effect, because the stress times are much smaller in these plots and, hence, the number of trapped charges that can be emitted during the measurement windows are much smaller. Consequently, the results are less statistically significant and larger discrepancies between the experimental data and the fitted model are to be expected.

The results above have been obtained for the bivariate lognormal distribution in (2). However, the procedure is fully general and can be applied to any other distribution. For the sake of illustration, Fig. 5 shows the fitting results where an identical procedure is applied with a log-uniform distribution. It can be seen that the fitting to the experimental results is considerably worse in this case.

TABLE II  
PARAMETERS EXTRACTED FOR THE CET MAP DISTRIBUTION

$\mu_{t_e}^*$	$\mu_{t_c}^*$	$\sigma_{t_e}^*$	$\sigma_{t_c}^*$	$\rho^*$	$\beta_e (V^{-1})$	$\beta_c (V^{-1})$
0.43	4.19	2.64	9.80	0.5	1.53	-2.40

\* As these correspond to parameters of the bivariate lognormal distribution, time constants have been normalized to 1s before applying the logarithm. Decimal logarithm has been used in these parameters.

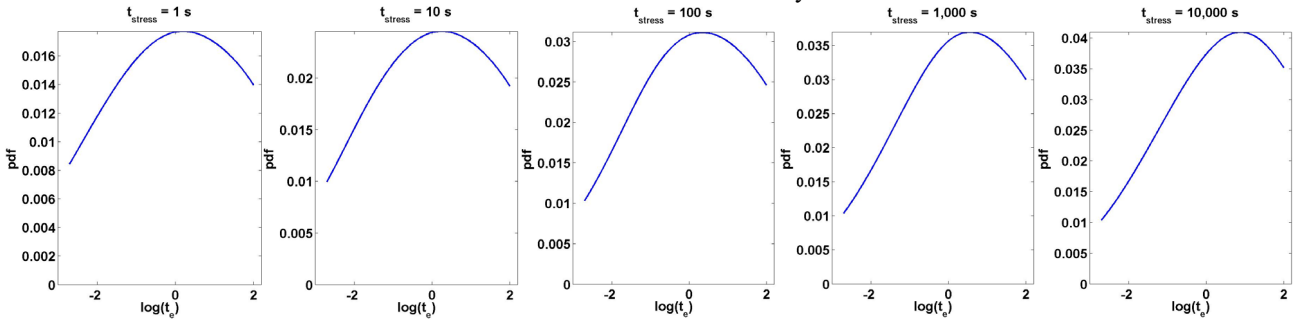


Fig. 4. Representation of (11) for the 5 SM cycles.

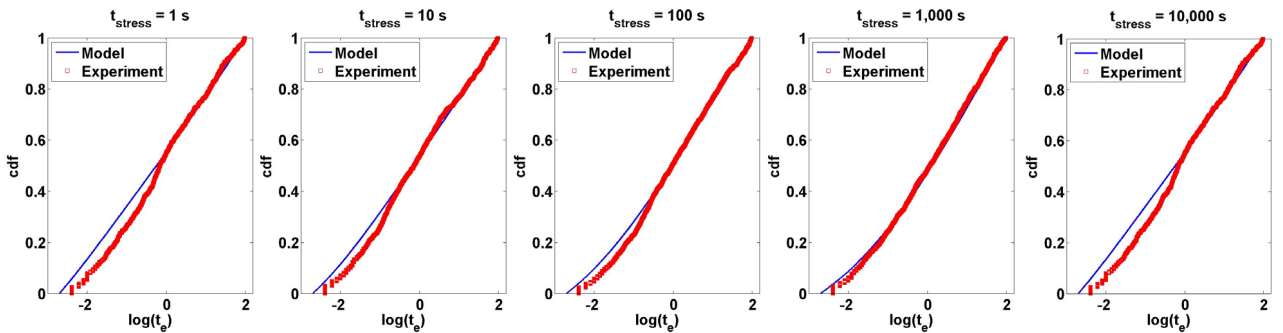


Fig. 5. Comparison of cdf of time of SEEs detected for 600 devices stressed at  $|V_{gs}| = 2.5V$ , for a recovery phase of 100s, and the representation of the cdf for the 5 SM cycles using a bivariate log-uniform distribution.

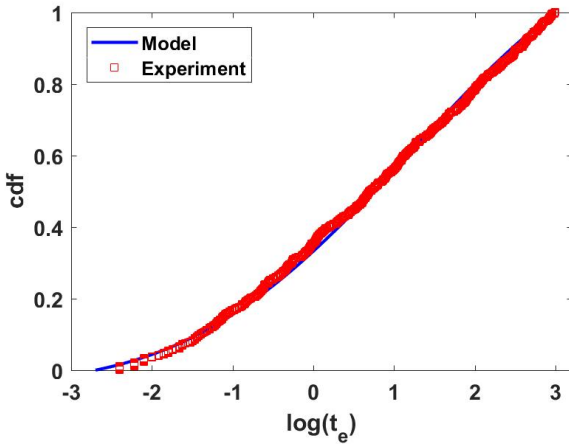


Fig. 6. Comparison of predicted SEE distribution (blue curve) for a recovery phase of 1,000s at  $|V_{gs}| = 0.6V$  after a stress phase of 100,000s at  $|V_{gs}| = 2.5V$  vs. the experimental measurements at the same conditions (red symbols).

The quality of the fitting process can also be evaluated by comparing the behavior predicted by the defect-centric model and the model parameters in Table II, with the results obtained in the laboratory for measurement conditions that were not used for model fitting, spanning the duration of both stress and measurement phases. In particular, a set of 200 pristine PMOS devices of  $W=80nm$  and  $L=60nm$  has been considered. These 200 devices were subjected to a stress voltage of  $|V_{gs}| = 2.5V$  during 100,000s and the recovery of each device was measured during the first 1,000s. The corresponding cdf of the time-to-emission is shown with red symbols in Fig. 6. On the other hand, the defect density function in (2) was computed for the model parameters in Table II. The solution of equation (4) was used to calculate the probability of occupation at the end of the 100,000s of stress phase. And, finally, equation (9) was used to compute the probability that a SEE occurs between 2ms and 1,000s. The multiplication of these three probabilities and integration over all possible values of emission and capture time constants, as in equation (11), yields the predicted probability density function of the times-to-emission of the SEEs. Fig. 6 shows the comparison between the cdf of the experimental results obtained in the laboratory (red symbols) and the cdf of the predicted values using the model parameters in Table II (blue curve). It can be observed that the fitting result is quite good despite the fact that due to the longer stress and recovery times only 200 devices were stressed in the lab, and, hence, the number of experimental distribution samples is considerably smaller, which reinforces the adequacy of the fitting procedure presented in this work.

Notice that the fitting procedure reported here is appropriate for small enough FETs, i.e., devices where charge de-trapping during the recovery phase is observed as sudden changes in current. As such behavior has been described for other 65nm technologies and below (see for instance, 45nm and 65nm bulk CMOS in [22], 28nm in [23], 8nm and 7nm FinFET in [24]), it is quite reasonable to state that the work can be readily adopted for 65nm technologies and below. As for the upper limit,

though this would depend on the particular technology, it could be around 100nm in width and length. For larger devices, the number of defects is so high that the recovery traces obtained using an MSM characterization procedure are smooth curves and the time-to-emissions of SEEs can be hardly detected. The same consideration applies in older technologies, i.e., with channel lengths around 100nm and above. Nevertheless, although the fitting procedure involves the characterization of small transistors, the fitted model can also be applied to larger transistors since the behavior can be simulated as the collective contribution of a larger number of defects in each device.

## V. CONCLUSIONS

Defect-centric models have been proposed to deal with the TDV observed in nanometric FET technologies. Although such models are fundamental to predicting the impact of TDV phenomena on circuits, their full and detailed determination has been often overlooked. As shown in this paper, going from experimental data to an accurate and trustworthy model is neither straightforward nor simple. To tackle this problem, this paper presents a detailed step-by-step procedure to construct a defect-centric model that allows retrieving the time constants associated with the defects by exploiting the experimental data from typical MSM tests. Unlike other approaches based on defect tracking and averaged time constants, the proposed method directly fits the distribution functions to the observed time-to-emissions, efficiently exploiting all experimental data obtained in the laboratory.

## REFERENCES

- [1] V. M. Van Santen, J. Martin-Martinez, H. Amrouch, M. Nafria, J. Henkel, "Reliability in super- and near-threshold computing: A unified model of RTN, BTI, and PV", *IEEE Transactions on Circuits and Systems I: Regular Papers*, vol. 65, no. 1, pp. 293-306, 2017.
- [2] T. Grasser, K. Rott, H. Reisinger, M. Waltl, J. Franco, B. Kaczer, "A unified perspective of RTN and BTI", In *IEEE International Reliability Physics Symposium (IRPS)*, pp. 4A-5, 2014.
- [3] J. Martin-Martinez, B. Kaczer, M. Toledano-Luque, R. Rodriguez, M. Nafria, X. Aymerich and G. Groeseneken, "Probabilistic defect occupancy model for NBTI". In: *2011 International Reliability Physics Symposium*. IEEE, 2011, XT-4.
- [4] S. Realov and K. L. Shepard, "Analysis of random telegraph noise in 45-nm CMOS using on-chip characterization system," *IEEE Transactions on Electron Devices*, vol. 60, no. 5, pp. 1716-1722, May 2013.
- [5] Z. Zhang, S. Guo, X. Jiang, R. Wang, Z. Zhang, P. Hao, Y. Wang and R. Huang, "New insights into the amplitude of random telegraph noise in nanoscale MOS devices," *IEEE International Reliability Physics Symposium (IRPS)*, 2017, pp. 3C-3.1-3C-3.5.
- [6] P. Saraza-Canflanca, J. Martin-Martinez, R. Castro-Lopez, E. Roca, R. Rodriguez, F. V. Fernandez and M. Nafria, "Statistical characterization of time-dependent variability defects using the maximum current fluctuation," *IEEE Transactions on Electron Devices*, vol. 68, no. 8, pp. 4039-4044, Aug. 2021.
- [7] H. Reisinger, T. Grasser, W. Gustin and C. Schl nder, "The statistical analysis of individual defects constituting NBTI and its implications for modeling DC- and AC-stress," *2010 IEEE International Reliability Physics Symposium*, 2010, pp. 7-15.
- [8] T. Grasser, H. Reisinger, P. Wagner, F. Schanovsky, W. Goes and B. Kaczer, "The time dependent defect spectroscopy (TDDS) for the characterization of the bias temperature instability," *2010 IEEE International Reliability Physics Symposium*, 2010, pp. 16-25.
- [9] T. Grasser, "Stochastic charge trapping in oxides: From random telegraph noise to bias temperature instabilities," *Microelectronics Reliability*, vol. 52, pp. 39-70, 2012.

- [10] H. Reisinger, T. Grasser, K. Ermisch, H. Nielen, W. Gustin and C. Schlünder, "Understanding and modeling AC BTI," 2011 International Reliability Physics Symposium, 2011, pp. 6A.1.1-6A.1.8.
- [11] G. Rzepa, W. Goes, G. Rott, K. Rott, M. Karner, C. Kernstock, B. Kaczer, H. Reisinger and T. Grasser, "Physical modeling of NBTI: From individual defects to devices," 2014 International Conference on Simulation of Semiconductor Processes and Devices (SISPAD), 2014, pp. 81-84.
- [12] K. Puschkarsky, H. Reisinger, C. Schlünder, W. Gustin and T. Grasser, "Voltage-dependent activation energy maps for analytic lifetime modeling of NBTI without time extrapolation," IEEE Transactions on Electron Devices, vol. 65, no. 11, pp. 4764-4771, Nov. 2018.
- [13] B. Kaczer, T. Grasser, J. Roussel, J. Martin-Martinez, R. O'Connor, B. J. O'Sullivan, G. Groeseneken, "Ubiquitous relaxation in BTI stressing—New evaluation and insights", In IEEE International Reliability Physics Symposium (IRPS), pp. 20-27, 2008.
- [14] J. Diaz-Fortuny, J. Martin-Martinez, R. Rodriguez, R. Castro-Lopez, E. Roca, X. Aragones, E. Barajas, D. Mateo, F. V. Fernandez, M. Nafria, "A versatile CMOS transistor array IC for the statistical characterization of time-zero variability, RTN, BTI and HCI", IEEE Journal of Solid-State Circuits, vol. 54, no. 2, pp. 476-488, 2018.
- [15] J. Diaz-Fortuny, P. Saraza-Canflanca, R. Castro-Lopez, E. Roca, J. Martin-Martinez, R. Rodriguez, F. V. Fernandez, M. Nafria, "Flexible setup for the measurement of CMOS time-dependent variability with array-based integrated circuits", IEEE Transactions on Instrumentation and Measurement, vol. 69, no. 3, pp. 853-864, March 2020.
- [16] P. Saraza-Canflanca, J. Diaz-Fortuny, R. Castro-López, E. Roca, J. Martín-Martínez, R. Rodríguez, M. Nafria, F. V. Fernández. "A robust and automated methodology for the analysis of Time-Dependent Variability at transistor level." Integration, the VLSI Journal, vol. 72 pp. 13-20, 2020.
- [17] T. Grasser, P.-J. Wagner, H. Reisinger, Th. Aichinger, G. Pobegen, M. Nelhiebel, B. Kaczer, "Analytic modeling of the bias temperature instability using capture/emission time maps," IEEE International Electron Devices Meeting, 2011, pp. 27.4.1-27.4.4.
- [18] P. Saraza-Canflanca, J. Martin-Martinez, R. Castro-Lopez, E. Roca, R. Rodriguez, M. Nafria and F. V. Fernandez, "A detailed study of the gate/drain voltage dependence of RTN in bulk pMOS transistors", Microelectronic Engineering, vol. 215, p.111004, 2019.
- [19] M.J. Kirton, M.J. Uren, "Noise in solid-state microstructures: A new perspective on individual defects, interface states and low-frequency ( $1/f$ ) noise," Advances in Physics, 38:4, 367-468, 1989.
- [20] P. Weekx, B. Kaczer, J. Franco, Ph J. Roussel, E. Bury, A. Subirats, G. Groeseneken, F. Cathoor, D. Linten, P. Raghavan, A. Thean, "Defect-centric perspective of combined BTI and RTN time-dependent variability." In IEEE International Integrated Reliability Workshop (IIRW), pp. 21-28, 2015.
- [21] D. Wang, D. Tan, L. Liu, "Particle swarm optimization algorithm: an overview." Soft Computing, vol. 22, pp. 387-408, 2018.
- [22] L.M. Procel, F. Crupi, J. Franco, L. Trojman, B. Kaczer, N. Wils, H. Tuinhout, "A Defect-Centric perspective on channel hot carrier variability in nMOSFETs," Microelectronic Engineering, Volume 147, pp 72-74, 2015.
- [23] B. Kaczer, J. Franco, P. Weekx, Ph.J. Roussel, E. Bury, M. Cho, R. Degraeve, D. Linten, G. Groeseneken, H. Kukner, P. Raghavan, F. Cathoor, G. Rzepa, W. Goes and T. Grasser, "The defect-centric perspective of device and circuit reliability—From gate oxide defects to circuits," Solid-State Electronics, vol. 125, pp. 52-62, 2016.
- [24] H. Jiang, J. Kim, K. Choi, H. Shim, H. Sagong, J. Park, H. Rhee and E. Lee, "Time dependent variability in advanced FinFET technology for end-of-lifetime reliability prediction," IEEE International Reliability Physics Symposium (IRPS), pp. 1-6, 2021.